Magnetic damping modulation in $IrMn_3/Ni_{80}Fe_{20}$ via the magnetic spin Hall effect

José Holanda[1*], Hilal Saglam[1,2,3], Vedat Karakas[4], Zhizhi Zang[1,5], Yi Li[1], Ralu Divan[6], Yuzi Liu[6], Ozhan Ozatay[4], Valentine Novosad[1], John E. Pearson[1] and Axel Hoffmann[1,7]

[1]Materials Science Division, Argonne National Laboratory, Lemont, Illinois 60439, USA
[2]Illinois Institute of Technology, Chicago, Illinois 60616, USA
[3]Department of Applied Physics, Yale University, New Haven, Connecticut 06511, USA
[4]Physics Department, Bogazici University, North Campus, Bebek/Istanbul 34342, Turkey
[5]School of Optical and Electronic Information, Huazhong University of Science and Technology, Wuhan 430074, People's Republic of China
[6]Center for Nanoscale Materials, Argonne National Laboratory, Argonne, IL 60439, USA
[7]Department of Materials Science and Engineering, University of Illinois at Urbana-Champaign, Urbana, IL 61801, USA

Non-collinear antiferromagnets can have additional spin Hall effects due to the net chirality of their magnetic spin structure, which provides for more complex spin-transport phenomena compared to ordinary non-magnetic materials. Here we investigated how ferromagnetic resonance of permalloy ($Ni_{80}Fe_{20}$) is modulated by spin Hall effects in adjacent epitaxial $IrMn_3$ films. We observe a large dc modulation of the ferromagnetic resonance linewidth for currents applied along the [001] $IrMn_3$ direction. This very strong angular dependence of spin-orbit torques from dc currents through the bilayers can be explained by the magnetic spin Hall effect where $IrMn_3$ provides novel pathways for modulating magnetization dynamics electrically.

*Corresponding author: joseholanda.papers@gmail.com

Antiferromagnetic materials are promising for future spintronic applications, since they combine several advantages. They are robust against perturbation due to magnetic fields, produce no stray fields, display ultrafast dynamics, and are capable of generating large magnetotransport effects [1, 2]. The idea of using antiferromagnetic materials in spintronic devices [1-4] has gained interest with the realization that antiferromagnets can be efficient sources of spin currents [5-12] and that their spin structure can be modulated electrically. Furthermore, antiferromagnets with non-collinear spin configurations provide additional rich new spin-transport phenomena, since any chirality of their spin structure may result in non-vanishing Berry curvatures affecting profoundly their charge transport properties [13-15]. Towards this end, it has been shown that triangular antiferromagnets with chiral spin arrangements can exhibit ferromagnetic-like behaviors such as large anomalous Hall and Nernst effects, as well as a magneto-optical Kerr effect. An interesting addition to these discoveries is the magnetic spin Hall effect (MSHE) in the triangular antiferromagnet Mn_3Sn [16]. The origin of the MSHE is similar to that of the ordinary spin Hall effect (OSHE), however, the MSHE arises from a reactive counterpart of the dissipative spin response that gives rise to OSHE. This interpretation can be understood in terms of the symmetries of linear response functions that are supported here by the dependence of the spin Hall effect (SHE) signals on the magnetic-order parameter reversal. This means that the MSHE can be explored under the condition of ferromagnetic resonance and represents a new way of analyzing the magnetization dynamics, *i.e.*, when *dc* electrical current passes through the uniformly magnetized material, a non-equilibrium distribution of spins at the interface influences the dynamic properties. In particular, current-induced modulation of damping has become a standard technique for quantifying spin Hall effects [17, 18]. Therefore, the control of damping in ferromagnetic/antiferromagnetic bilayers can provide fundamental insights for ferromagnetic or antiferromagnetic spintronics.

An interesting material to be investigated is the non-collinear antiferromagnet $IrMn_3$, in which Mn atoms form Kagome lattice in the {111} planes [See **Fig. 1 (a)**]. $IrMn_3$ has a giant magnetocrystalline anisotropy energy due to the locally broken cubic symmetry of the Mn sublattices [19]. Additionally, $IrMn_3$ has a large variation of the spin Hall conductivities along different crystallographic orientations [20-22]. In this letter, we perform ferromagnetic resonance measurements without and with *dc* current in $IrMn_3/Ni_{80}Fe_{20}$ bilayers. Our results show a strong angular dependence of the electric current induced modulation of the ferromagnetic resonance

linewidth for magnetic fields applied along different crystalline orientations, *i.e.*, [001] and [011]. We report a maximum Gilbert damping modulation of 41% and the observed anisotropy for the magnetic fields applied along the two different crystalline directions can be associated with the variation of spin accumulation at the interface due to the additional contributions arising from the magnetic spin Hall effect.

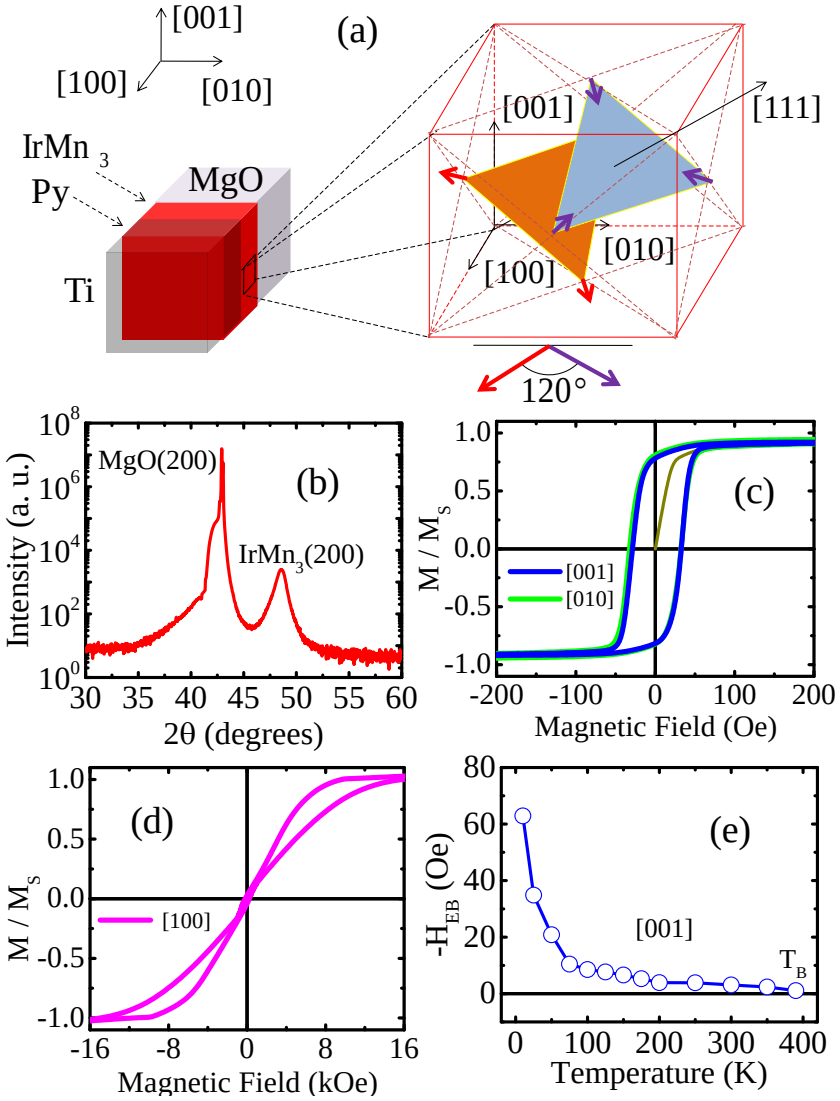

Figure 1: (a) shows the schematic of $IrMn_3/Ni_{80}Fe_{20}$ (permalloy, Py) bilayer capped with a thin layer of Ti and also includes the unit cell of $IrMn_3$ with its spin structure. Note that the Mn atoms in the unit cell of $IrMn_3$ form a Kagome lattice in the {111} planes with the spins either pointing in wards or outwards in each triangular Mn arrangement. **(b)** The X-ray diffraction pattern measured for a 20-nm thick $IrMn_3$ layer capped with a 2-nm Ti layer. **(c)** Measured magnetic

hysteresis curves after field-cooling in a magnetic field of +70 kOe applied along either [001] or [010] directions at a temperature of 300 K. **(d)** Magnetic hysteresis curves after field-cooling in a magnetic field of +70 kOe applied along the [100] direction at a temperature of 300 K. **(e)** Measured exchange bias field as a function of temperature after field cooling with an applied magnetic field of +70 kOe along the [001] direction, showing that the blocking temperature of $IrMn_3$(20 nm)/$Ni_{80}Fe_{20}$(10 nm) bilayer is 380 K.

We have grown nominally 20-nm thick epitaxial $IrMn_3$ films on MgO (100)-oriented single-crystal substrates at 843 K using a magnetron sputtering technique. Subsequently, a thin layer of $Ni_{80}Fe_{20}$(10 nm) and Ti(2 nm) were deposited at room temperature. Here, the Ti layer was used to protect the surface properties of $Ni_{80}Fe_{20}$. **Figure 1(a)** shows the unit cell of $IrMn_3$, where the Mn moments are parallel to the {111} planes and aligned along the <112> directions. **Figure 1(b)** shows an X-ray diffraction pattern for $IrMn_3$ grown on an MgO substrate. We found that $IrMn_3$ has a lattice constant of (0.377 ± 0.001) nm, which is consistent with previous literature values [20, 23].

The magnetic characterization was performed with a Superconducting Quantum Interference Device (SQUID) magnetometer. **Figures 1(c)**, **(d)** and **(e)** are measured for MgO/$IrMn_3$(20 nm)/$Ni_{80}Fe_{20}$(10 nm)/Ti(2 nm). In **Figures 1(c)** and **(d)** we show the hysteresis curves at room temperature (300 K) after field-cooling starting at temperature of 390 K with a magnetic field of +70 kOe applied along the crystallographic directions [001], [010] and [100]. From the SQUID measurements we also determine a saturation magnetization of M_S = (774±8) emu/cm^3, which is consistent with typical values reported for permalloy [16]. **Figure 1(e)** shows the exchange bias field as a function of temperature for magnetic fields applied along the [001] direction, where exchange bias is defined as $H_{EX} = -(H_1 + H_2)/2$. This means that the blocking temperature is above 300 K, which shows that $IrMn_3$ is antiferromagnetically ordered at room temperature [23].

We utilize a flip-chip ferromagnetic resonance technique [24] for characterizing the Gilbert damping measured for fields applied in different crystal orientations. We measured the transmission coefficient by sweeping the frequency at fixed fields. **Figure 2(a)** shows the experimental configuration for ferromagnetic resonance measurements without and with *dc* currents. **Figures 2(b)** and **(e)** show the ferromagnetic resonance (FMR) signals obtained with a

vector network analyzer (VNA) for magnetic fields applied along the [001] and [011] crystallographic directions, respectively. For the measurements with the magnetic field along [011] the sample is rotated 45° with respect to the coplanar waveguide and thus not symmetrically positioned, which may give rise to the slight asymmetric lineshape observed in **Figure 2(e)**.

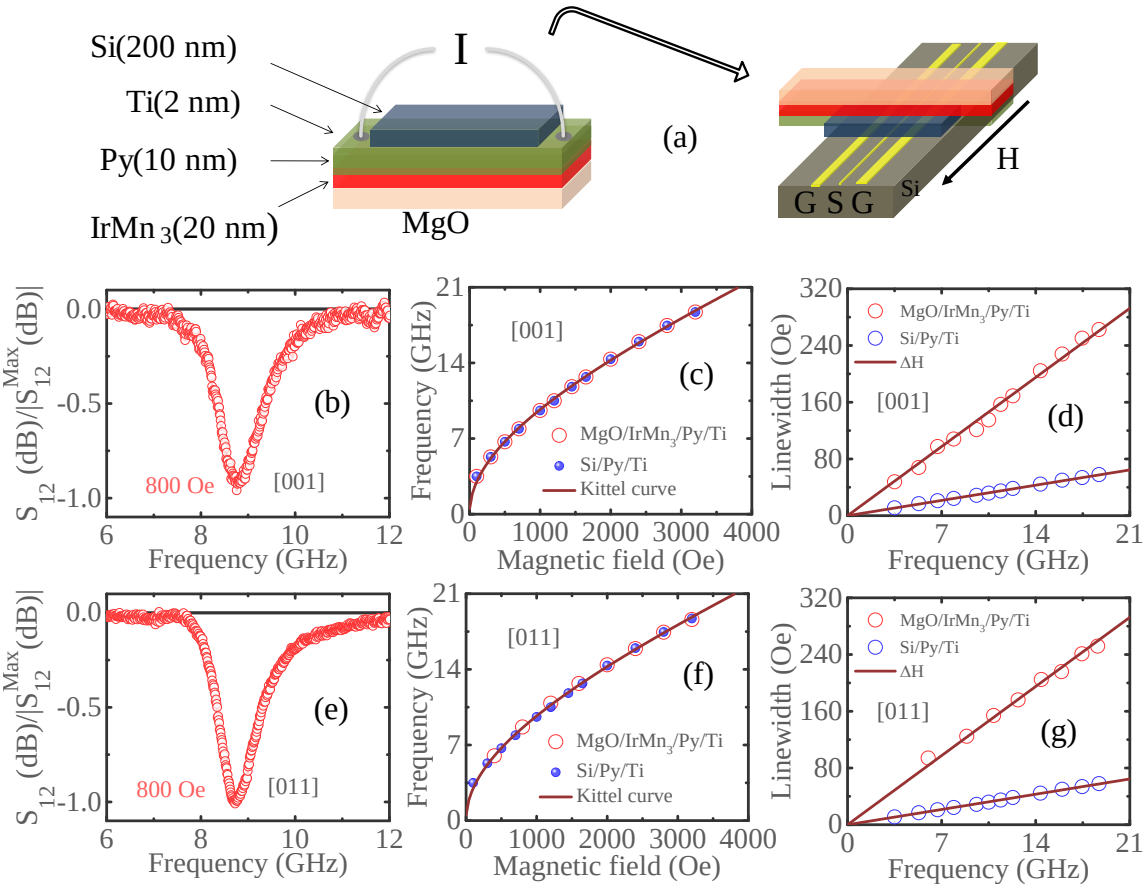

Figure 2: (a) Schematic of the flip-chip ferromagnetic resonance measurement set up, where *dc* current (I) leads are connected to the Ti layer. **(b)** and **(e)** ferromagnetic resonance (FMR) signals obtained using a VNA for the magnetic field applied along the [001] and [011] crystallographic directions, respectively. **(c)** and **(f)** FMR frequency as a function of magnetic field, which was applied along the [001] and [011] crystallographic directions, respectively. The fits are performed with the Kittel equation, where $\gamma = g\mu_B/\hbar = 2.8$ GHz/kOe and $4\pi M_{eff} = (9706 \pm 1)$ Oe. **(d)** and **(g)** show the linewidth variation as a function of the FMR frequency for the crystallographic directions [001] and [011], respectively.

Figures 2(c) and **(f)** show the measured FMR frequency as a function of the magnetic field. The solid curve is a fit of the experimental data to the Kittel equation, $f = \gamma[(H_R)(H_R + 4\pi M_{eff})]^{1/2}$ where $\gamma = g\mu_B/\hbar = 2.8$ GHz/kOe is the gyromagnetic ratio, g = 2 is the spectroscopic splitting factor, μ_B is the Bohr magneton, $\hbar$ the reduced Planck constant, and $4\pi M_{eff}$ the effective magnetization, which is determined by the fit $4\pi M_{eff}$ = (9706± 1) Oe, consistent with the SQUID data. As expected, there is no significant variation in the ferromagnetic resonance field for single $Ni_{80}Fe_{20}$ or $Ni_{80}Fe_{20}/IrMn_3$ samples. The frequency swept linewidths (Δf_{VNA}) were obtained via Lorentz fitting. Detailed steps, including the conversion from Δf_{VNA} to resonance magnetic field linewidth ΔH can be found in Ref. 24. The linewidth as a function of the frequency is given by $\Delta H = (\alpha/\gamma)f$ [25], where α is the magnetic Gilbert damping of the material. **Figures 2(d)** and **(g)** show the linewidth and fits are made using $\Delta H = (\alpha/\gamma)f$. The damping values for both crystallographic directions [001] and [011] are practically the same $\alpha_{IrMn_3/Py}$ = (3.94±0.02)×10^{-2} but damping increased significantly in comparison to a single layer of $Ni_{80}Fe_{20}$(Py) α_{Py} = (8.66±0.03)×10^{-3}. Using the variation of the damping, it is possible to determine the spin-mixing conductance $g_{eff}^{\uparrow\downarrow}$ = $4\pi M_{eff} t_{FM} \Delta\alpha/(\gamma\hbar)$= (1.6±0.1)×$10^{16}$$cm^{-2}$[19], where t_{FM} = 10 nm is the thickness of the ferromagnetic material ($Ni_{80}Fe_{20}$, Py).

The experimental results with applied dc currents along the [001] direction are shown in **Figure 3** and suggest that there are three distinct contributions to α: the first, current-independent mechanism is that α is strongly facet-dependent and is derived from the antiferromagnetic domains of the uncompensated spins; the second, magnetic field-independent mechanism is that it is facet-independent and arises from bulk spin-orbit coupling within the $IrMn_3$ layer, and the third mechanism, which is both magnetic field direction and electric current dependent, is the magnetic spin Hall effect (MSHE). It is known that chemically ordered $IrMn_3$ has a triangular chiral magnetic structure with the Mn magnetic moments aligned at 120º to each other in the (111) plane [20]. The coupling of the magnetization of $Ni_{80}Fe_{20}$ to the Mn interface moments becomes strongly fixed in its preferred direction [26-28] by the preferred antiferromagnetic domains in the bulk of the $IrMn_3$ film. The coupling at the $IrMn_3/Ni_{80}Fe_{20}$ interface is responsible for the spin current flow and the concomitant manipulation of damping of the magnetization in $Ni_{80}Fe_{20}$. **Figures 3(a)** and **(c)** show the linewidth variation as a function of the resonance frequency for the magnetic field applied along the [001] and [011] crystallographic directions, respectively. Based on the Landau-Lifshitz-Gilbert-Slonczewski equation the linewidth as a

function of the frequency can be written as $\Delta H = \alpha f/\gamma + \theta_{MSH}^{eff}\hbar j_c L/(2eM_{eff}\,t_{FM})$, where θ_{MSH}^{eff} is the effective magnetic spin Hall angle, e is the charge of electron, j_c is the charge density and the spin transparency of interface is represented by $L = \left[g_{eff}^{\uparrow\downarrow}\tan(t_{AF}/2\lambda_{AF})\right]/\left[\sigma h/(2\lambda_{AF}e^2) + g_{eff}^{\uparrow\downarrow}\coth(t_{AF}/\lambda_{AF})\right]$[29], where λ_{AF} is the spin diffusion length in the $IrMn_3$, $g_{eff}^{\uparrow\downarrow}$ is the effective spin mixing conductance, σ is the electrical conductivity and t_{AF} is the thickness of the $IrMn_3$. For analyzing the measurements of the $IrMn_3$(20 nm)/Py(10 nm) samples with the magnetic field applied along the [001] direction we used the following parameters: resonance frequency f = (17.45 ± 0.03) GHz, linewidth of ΔH = (336.5 ± 0.5) Oe, *dc* current density of $j_c = 2.5\times 10^4 Acm^{-2}$, the spin diffusion length λ_{AF} = 1 nm [20], thickness t_{AF} = 20 nm, and electrical conductivity $\sigma_{[001]}^{Elec}$ = (8.2 ± 0.2)×10^3 $\Omega^{-1}cm^{-1}$, which is in accordance with the previously reported values [20-22]; using these parameters we obtain an effective magnetic spin Hall angle of θ_{MSH}^{eff} ~ (0.33 ± 0.02). This result is consistent with Ref. 20, where the spin Hall effect was probed via other techniques.

We observe that for the magnetic field applied along the [001] direction a change in the magnetic damping occurs, depending on the direction (positive or negative) of the applied *dc* current. This does not occur when the magnetic field is applied along the [011] direction, which indicates a change of the current induced toques in $Ni_{80}Fe_{20}$ as a function of the magnetic field due to the MSHE of $IrMn_3$. Also note that the electrical conductivity of $Ni_{80}Fe_{20}$ is $\sigma_{Py} = 2\times 10^4 \Omega^{-1}cm^{-1}$ [30] and thus $\sigma_{Py}/\sigma_{[001]}^{Elec}$ = (2.4 ± 1). Together with the thickness ratio of the two layers, this means that the *dc* current flows in about equal parts through the $Ni_{80}Fe_{20}$ and $IrMn_3$ layers. At the same time $Ni_{80}Fe_{20}$ has a small spin Hall angle, θ_{SH} = 0.005 [31] compared to $IrMn_3$ (*i.e.*, $\theta_{SH}/\theta_{MSH}^{eff} \approx$ 1.5%) and thus any magnetic torques originating from electric current flowing through the $Ni_{80}Fe_{20}$ layer can be neglected. **Figures 3(b)** and **(d)** show the variation of the magnetic damping of the $Ni_{80}Fe_{20}$ layer as a function of the applied *dc* current along the crystallographic [001] direction and the magnetic field applied in crystallographic [001] and [011] directions, respectively.

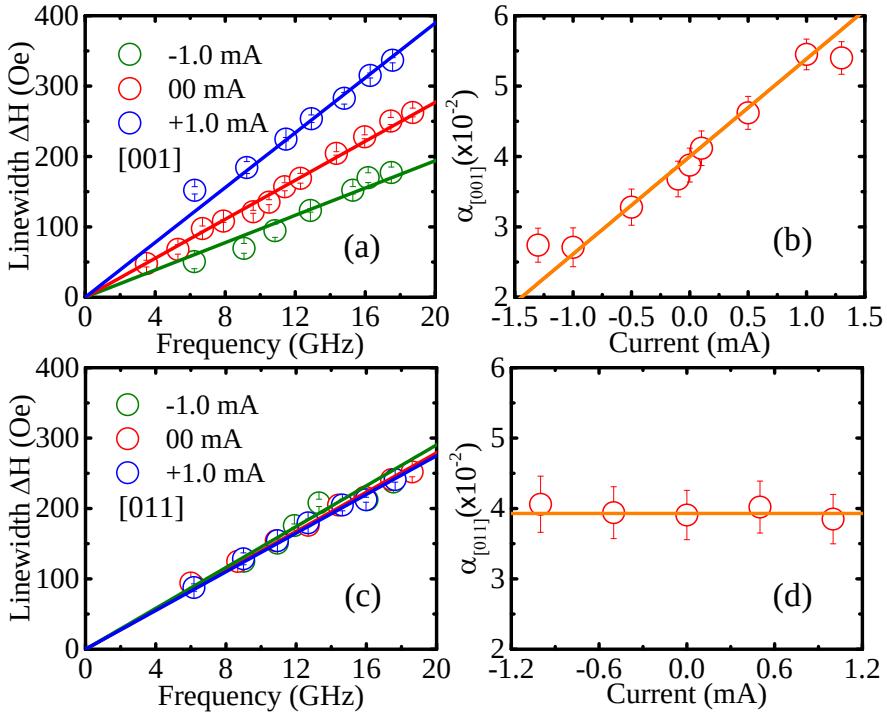

Figure 3: Electric current modulation of FMR measured for MgO/$IrMn_3$(20 nm)/$Ni_{80}Fe_{20}$(10 nm)/Ti(2 nm). **(a)** and **(c)** FMR linewidth variation as a function of the resonance frequency with *dc* currents of ±1 mA applied along the [001] crystallographic direction and magnetic field applied along the [001] and [011] crystallographic directions, respectively. **(b)** and **(d)** damping variation as a function of *dc* current for the [001] and [011] crystallographic directions, respectively.

The MSHE generated in $IrMn_3$ leads to significant changes in the magnetization dynamics of the adjacent $Ni_{80}Fe_{20}$ layer depending on the crystalline orientations. For a (100)-oriented $IrMn_3$ film, the in-plane current leads to a large out-of-plane spin current whose amplitude is much larger than that of a (111)-oriented $IrMn_3$ films [20]. In $IrMn_3$, the Mn atoms are arranged in the form of triangles within the {111} planes of the primitive crystallographic unit cell, such that the Mn moments point either toward (spins-in) or away from the center of the triangle (spins-out), respectively [see **Fig. 4 (a)**]. Using either a mirror reflection or time-reversal operation, the spins-in and spins-out configurations can be transformed into each other. For example, for the (011)-crystallographic plane, the reversal operation process should apply to both

the lattice and the magnetic moments and thus time-reversal reverses the directions of all moments, because either the mirror symmetry or the time-reversal symmetry is broken in $IrMn_3$. On the other hand, spins-in and spins-out are nonequivalent ground states and are chiral images of each other. In this case, the spins-in and spins-out configurations exhibit the same energies and both exist spontaneously in the material [32, 33]. It is known that under time reversal the magnetic spin Hall effect is odd [16], whereas the conventional spin Hall effect is even [31]. Thus, we can conclude with the help of time reversal that both spin configurations will exhibit the same MSHE, as schematically shown in **Fig. 4**.

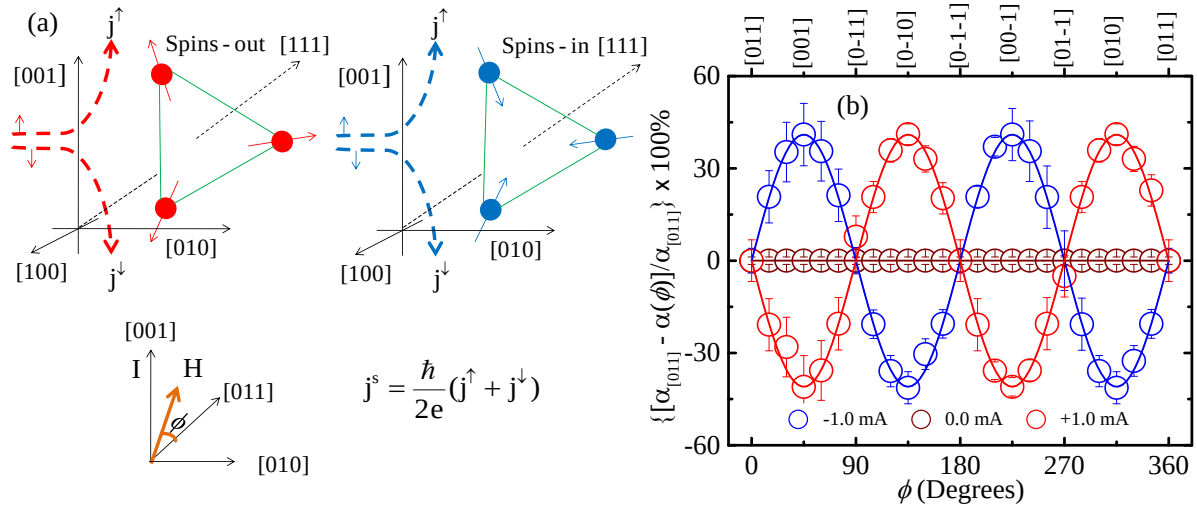

Figure 4: (a) Schematic diagram of two chiral antiferromagnetic spin configurations (spins-in and spins-out) of the Mn moments in $IrMn_3$. Due to the magnetic spin Hall effect, the trajectories of spin-up and spin-down electrons have opposite transverse components and produce a spin current in the [001] direction. The angular variation of the magnetic field (H) in the plane of the film is also shown and it determines the polarization of the spin accumulation due to magnetic spin Hall effect. **(b)**Variation of the current dependent Gilbert magnetic damping as a function of the applied magnetic field angle, which in turn defines the polarization of the spin accumulation due to magnetic spin Hall effect. The curves represent the function $\{[\alpha_{[011]} - \alpha(\phi)]/\alpha_{[011]}\}\times 100\% = \Delta\alpha_{MSHE} \sin(\pm 2\phi)$, with $\Delta\alpha_{MSHE} = (40 \pm 1)$ %.

Figure 4(b) shows for a $MgO/IrMn_3(20nm)/Ni_{80}Fe_{20}(10nm)/Ti(2nm)$ sample the damping variation as a function of the applied magnetic field angle, which in turn defines the

polarization of the spin accumulation due to the magnetic spin Hall effect. The modulation of the electric current induced damping modulation of the $Ni_{80}Fe_{20}$ as a function of the applied magnetic field direction provides an efficient pathway for modulating magnetization dynamics. The influence of the spin accumulation generated by the spin current $j^s = (j^{\uparrow} + j^{\downarrow})\hbar/2e$ at the antiferromagnetic/ferromagnetic interface due to the MSHE also depends on the crystallographic direction of the material. As shown in **Fig. 3(a)** for -1 mA or +1 mA *dc* current, the damping variation for magnetic fields applied either along the [001] or [011] crystallographic directions is $\Delta\alpha_{MSHE} \approx (40\pm1)\%$. This result was also confirmed by the data in **Fig. 4 (b)**. The fit of **Fig. 4 (b)** was realized with the function $\{[\alpha_{[011]} - \alpha(\phi)]/\alpha_{[011]}\}\times100\% = \Delta\alpha_{MSHE} \sin(\pm2\phi)$, where $\Delta\alpha_{MSHE} = (40\pm1)\%$. A variation of this order opens new possibilities for the control of spin currents and thus information flow in spintronics devices. The fact that we observe an even field dependence of the damping modulation with electric currents indicates that the mirror symmetry is broken in $IrMn_3$, which gives rise to the MSHE in this material [16]. In other words, the MSHE is influenced by the contributions of intrinsic Hall conductivities of the domains with opposite chirality of spin [34].

Similar measurements were performed with *dc* electrical currents applied along the [011] crystallographic direction. The results are similar to the ones shown in **Figure 4(b)**. It is also worthwhile to note that recently very large anisotropies of the magnetization damping as a function of magnetic field direction with respect to the crystalline orientation have been observed for individual ferromagnetic layers [35]. This differs from the current observation where the magnetic damping of the $Ni_{80}Fe_{20}$ film without any applied electric current is largely independent of the magnetic field orientation as can be seen in **Figs. 3(b)** and **(d)**. In contrast here, only the electric current dependent part of the magnetization damping shows a large anisotropy.

In summary, we have shown that bilayers of $IrMn_3/Ni_{80}Fe_{20}$ have a strong modulation of electric current induced damping-like spin torques. The angular magnetic field dependence indicates that these damping-like torques originate from magnetic spin Hall effects in the $IrMn_3$. This indicates that chiral antiferromagnetic systems, such as $IrMn_3$ can provide additional functionality for electric current control of magnetization dynamics with very different symmetries than what can be expected from conventional spin Hall effects. Thus, this work provides new perspectives for the fundamental understanding of charge- to spin-current

conversions in antiferromagnets, as well as new avenues for integrating chiral antiferromagnets into spintronics devices.

Acknowledgments

We acknowledge useful discussion with Roland Winkler. All experimental work was performed at the Argonne National Laboratory and supported by the Department of Energy, Office of Science, Materials Science and Engineering Division. The use of the Centre for Nanoscale Materials was supported by the U. S. Department of Energy (DOE), Office of Sciences, Basic Energy Sciences (BES), under Contract No. DE-AC02-06CH11357. Part of the data analysis was also supported by the NSF through the University of Illinois at Urbana-Champaign Materials Research Science and Engineering Center DMR-1720633. José Holanda acknowledges financial support from Conselho Nacional de Desenvolvimento Científico e Tecnológico (CNPq)-Brasil. Vedat Karakas and Ozhan Ozatay acknowledge financial support from TUBITAK grant 118F116 and Bogazici University Research Fund grant 17B03D3. Zhizhi Zhang acknowledges additional financial support from the China Scholarship Council (no. 201706160146) for a research stay at Argonne.

References

[1] V. Baltz, A. Manchon, M. Tsoi, T. Moriyama, T. Ono, and Y. Tserkovnyak. Antiferromagnetic spintronics. Rev. Mod. Phys. **90**, 015005 (2018).

[2] M. B. Jungfleisch, W. Zhang, A. Hoffmann. Perspectives of antiferromagnetic spintronics. Physics Letters A, **382,** 865 (2018).

[3] S. M. Rezende, A. Azevedo, and R. L. Rodríguez-Suárez. Introduction to antiferromagnetic magnons. J. Appl. Phys. **126**, 151101 (2019).

[4] J. Zelezný, P. Olejník, A. Hoffmann and H. Ohno. Spin transport and spin torque in antiferromagnetic devices. Nature Phys. **14**, 220 (2018).

[5] W. Zhang, M. B. Jungfleisch, W. Jiang, J. E. Pearson, and A. Hoffmann. Spin Hall effects in metallic antiferromagnets. Phys. Rev. Lett. **113**, 196602 (2014).

[6] S. Seki, T. Ideue, M. Kubota, Y. Takagi, M. Nakamura, Y. Kaneko, M. Kawasaki, and Y. Tokura. Thermal generation of spin current in an antiferromagnet. Phys. Rev. Lett. **115**, 266601 (2015).

[7] S. M. Wu, W. Zhang, A. KC, P. Borisov, J. E. Pearson, J. S. Jiang, D. Lederman, A. Hoffmann, and A. Bhattacharya. Antiferromagnetic spin Seebeck effect. Phys. Rev. Lett. **116**, 097204 (2016).

[8] J. Holanda, D. S. Maior, O. Alves Santos, L. H. Vilela-Leao, J. B. S. Mendes, A. Azevedo, R. L. Rodríguez-Suárez, and S. M. Rezende. Spin Seebeck effect in the antiferromagnet nickel at room temperature. Appl. Phys. Lett. **111**, 172405 (2017).

[9] F. L. A. Machado, P. R. T. Ribeiro, J. Holanda, R. L. Rodríguez-Suárez, A. Azevedo, and S. M. Rezende. Spin-flop transition in the easy-plane antiferromagnet nickel oxide. Phys. Rev. B **95**, 104418 (2017).

[10] P. Wadley, B. Howells, J. Železný, C. Andrews, V. Hills, R. P. Campion, V. Novák, K. Olejník, F. Maccherozzi, S. S. Dhesi, S. Y. Martin, T. Wagner, J. Wunderlich, F. Freimuth, Y. Mokrousov, J. Kuneš, J. S. Chauhan, M. J. Grzybowski, A. W. Rushforth, K. W. Edmonds, B. L. Gallagher, T. Jungwirth. Electrical switching of an antiferromagnet. Science **351**, 587 (2016).

[11] H. Saglam, J. C. Rojas-Sanchez, S. Petit, M. Hehn, W. Zhang, J. E. Pearson, S. Mangin, and A. Hoffmann. Independence of spin-orbit torques from the exchange bias direction in $Ni_{81}Fe_{19}$/IrMn bilayers. Phys. Rev. B **98**, 094407 (2018).

[12] J. E. Hirsch. Spin Hall effect. Phys. Rev. Lett. **83**, 1834 (1999).

[13] S. Nakatsuji, N. Kiyohara, T. Higo. Large anomalous Hall effect in a non-collinear antiferromagnet at room temperature. Nature **527**, 212 (2015).

[14] A. K. Nayak, J. E. Fischer, Y. Sun, B. Yan, J. Karel, A. C. Komarek, C. Shekhar, N. Kumar, W. Schenelle, J. Kubler, S. S. P. Parkin, C. Felser. Large anomalous Hall effect driven by a nonvanishing Berry curvature in the non-collinear antiferromagnet Mn_3Ge. Sci. Adv. **2**, e1501870 (2015).

[15] R. Shindou and N. Nagaosa. Orbital ferromagnetism and anomalous Hall effect in antiferromagnets on the distorted fcc lattice. Phys. Rev. Lett. **87**, 116801 (2001).

[16] M. Kimata, H. Chen, K. Kondou, S. Sugimoto, P. K. Muduli, M. Ikhlas, Y. Omori, T. Tomita, A. H. MacDonald, S. Nakatsuji and Y. Otani. Magnetic and magnetic inverse spin Hall effects in a non-collinear antiferromagnet. Nature **565**, 627 (2019).

[17] K. Ando, S. Takahashi, K. Harii, K. Sasage, J. Ieda, S. Maekawa, and E. Saitoh. Electric manipulation of spin relaxation using the spin Hall effect. Phys. Rev. Lett. **101**, 036601 (2008).

[18] L. Liu, T. Moriyama, D. C. Ralph, and R. A. Buhrman. Spin-torque ferromagnetic resonance induced by the spin Hall effect. Phys. Rev. Lett. 106, 036601 (2011).

[19] L. Szunyogh, B. Lazarovits, L. Udvardi, J. Jackson, U. Nowak. Giant magnetic anisotropy of the bulk antiferromagnets IrMn and $IrMn_3$ from first principles. Phys. Rev. B – Condens. Matter. Mater. Phys. **79**(2), 1 (2009).

[20] W. Zang, W. Han, S.-H. Yang, Y. Sun, Y. Zhang, B. Yan, S. S. P. Parkin. Giant facet-dependent spin-orbit torque and spin Hall conductivity in the triangular antiferromagnet $IrMn_3$. Sci. Adv. **2**, e1600759 (2016).

[21] H. Chen, Qian Niu, A. H. MacDonald. Anomalous Hall effect arising from non-collinear antiferromagnetism. Phys. Rev. Lett. **112**, 017205 (2014).

[22] M. Seemann, D. Kodderitzsch, S. Wimmer, H. Ebert. Symmetry-imposed shape of linear response tensors. Phys. Rev. B **92**, 155138 (2015).

[23] A. Kohn, A. Kovács, R. Fan, G. J. Mclntyre, R. C. C. Ward and J. P. Goff. The antiferromagnetic structures of $IrMn_3$ and their influence on exchange-bias. Scientific Reports **3**, 7 (2013).

[24] J. Holanda, O. Alves Santos, R. L. Rodríguez-Suárez, A. Azevedo, S. M. Rezende, Simultaneous spin pumping and spin Seebeck experiments with thermal control of the magnetic damping in bilayers of yttrium iron garnet and heavy metals: YIG/Pt and YIG/IrMn, Physical Review **B 95**, 134432 (2017).

[25] T. L. Gilbert. A phenomenological theory of damping in ferromagnetic materials. IEEE Trans. Magn. **40**, 3443 (2004).

[26] W. Zhang, W. Han, X. Jiang, S.-H. Yang and S. S. P. Parkin. Role of transparency of platinum-ferromagnet interfaces in determining the intrinsic magnitude of the spin Hall effect. Nature Phys. **11**, 496 (2015).

[27] M. Tsunoda, T. Sato, T. Hashimoto, and M. Takahashi. Exchange anisotropy of polycrystalline Mn-Ir/Co-Fe bilayers enlarged by long-time annealing. Appl. Phys. Lett. **84**, 5222 (2004).

[28] C. G. Shull and M. K. Wilkinson. Neutron diffraction studies of various transition elements. Rev. Moder. Phys. **25**, 1 (1953).

[29] S. Maekawa, S. O. Valenzuela, E. Saitoh, T. Kimura. Spin current (Oxford Univ. Press, 2012).

[30] W. T. Soh, Y. Yeow, X. Zhong and C K Ong. Inverse spin Hall effect of antiferromagnetic MnIr in exchange biased NiFe/MnIr films. J. Phys. D. Appl. Phys. **48**, 345002 (2015).

[31] A. Tsukahara, Y. Ando, Y. Kitamura, H. Emoto, E. Shikoh, M. P. Delmo, T. Shinjo, and M. Shiraishi. Self-induced inverse spin Hall effect in permalloy at room temperature. Phys. Rev. B **89**, 235317 (2014).

[32] V. Hemmati, M. L. Plumer, J. P. Whitehead, and B. W. Southern. Monte Carlo simulations of magnetic ordering in the fcckagome lattice. Phys. Rev. B **86**, 104419 (2012).

[33] Y. Liu, Y. Liu, M.Chen, S. Srivastava, P. He, K. L. Teo, T. Phung, S.-H. Yang, and H. Yang. Current-induced out-of-plane spin accumulation on the (001) surface of the $IrMn_3$ antiferromagnet. Phys. Rev. Appl. **12**, 064046 (2019).

[34] Y. Zhang, Y. Sun, H. Yang, J. Zelezny, S. S. P. Parkin, C. Felser, and B. Yan. Strong anisotropic anomalous Hall effect and spin Hall effect in the chiral antiferromagnetic compounds Mn_3X (X = Ge, Sn, Ga, Ir, Rh, and Pt). Phys. Rev. B **95**, 075128 (2017).

[35] Y. Li, F. Zeng, S. S.-L. Zhang, H. Shin, H. Saglam, V. Karakas, O. Ozatay, J. E. Pearson, O. G. Heinonen, Y. Wu, A. Hoffmann, and W. Zhang. Giant anisotropy of Gilbert damping in epitaxial CoFe films. Phys. Rev. Lett. **122**, 117203 (2019).